Journal of Applied Electrochemistry (2006) 36:1057–1068
DOI 10.1007/s10800-006-9166-3

Electrochemical behaviour of retrogressed and reaged (RRA) 8090 and 1441 Al–Li–Cu–Mg–Zr alloys

K.S. GHOSH[1,*], K. DAS[2] and U.K. CHATTERJEE[2]
[1]*Department of Metallurgical and Materials Engineering, National Institute of Technology, Warangal, 506 004, India*
[2]*Department of Metallurgical and Materials Engineering, Indian Institute of Technology, Kharagpur, 721 302, India*
*(*author for correspondence, fax:+91-870-2459547, e-mail: ksghosh2001@yahoo.co.uk)*

Received 20 June 2005; accepted in revised form 5 June 2006

Key words: 8090 and 1441 Al–Li–Cu–Mg–Zr alloys, electrochemical polarisation, open circuit potential (OCP), peak and over aged tempers, retrogression and reaging (RRA)

Abstract

8090 and 1441 Al–Li–Cu–Mg–Zr alloys of peak aged T8 tempers were subjected to retrogression treatment followed by reageing to peak aged (RRA) T77 tempers. Electrochemical polarization studies were carried out on the alloys of T8, T77 and over aged T7 tempers, in 3.5% NaCl, 3.5% NaCl + 0.1M LiCl + 0.3% H_2O_2 and 3.5% NaCl + 0.1M LiCl + 0.7% H_2O_2 solutions. The shape of the polarization curves is similar for all the tempers of both alloys in all environments. The corrosion rates are more or less the same irrespective of the tempers. However, the open circuit potentials (OCP) shift towards more negative potential with the RRA treatment and ageing time. The OCP values of the T7 tempers were found to be the most negative; for the T77 tempers it lies between that of the T7 and T8. Further, the OCP values for all tempers of both alloys shifted anodically with addition of LiCl and H_2O_2 in 3.5% NaCl solution. TEM, XRD and DSC studies of microstructural features of the alloys in the T8, RRA and T7 tempers have been used to explain the observed electrochemical behaviour.

1. Introduction

The attractive combination of Al–Li alloys of 5–10% lower density, 15–25% increase in elastic modulus and 10–15% increase in specific strength over the most widely used aluminum alloys 2xxx and 7xxx series, has rendered them as candidate materials for aerospace applications [1–3]. In addition to being fuel efficient, aircraft structures are also required to exhibit an ability to resist environmental degradation caused by general or localized corrosion, stress corrosion cracking, hydrogen embrittlement and corrosion fatigue, for long service life. The presence of active element Li in Al–Li 8xxx series alloys gives different corrosion behaviour from conventional Al alloys. Most of the high strength aluminium alloys are susceptible to general and localized corrosion in NaCl solution. Further, the Al–Li alloys are also susceptible to environment induced cracking (EIC) [4–8].

Corrosion behaviour and electrochemical investigation have been carried out on Al–Li alloys by several investigators [9–13]. There are considerable differences in opinion between workers about the corrosion behaviour of these alloys. Ricker and Duquette [14] carried out potentiodynamic polarization studies with an Al–4.2Mg–2.1Li alloy and found an increased corrosion susceptibility compared with the 7050 (Al–6.5Zn–2.4Mg–2.2Cu) alloy. De Jong and Martens [15], who measured the pitting potential of rapidly solidified Al–Cu–Mg (–Li) alloys, reported the pitting potential to be slightly more negative with lithium additions. They observed no change of pitting potential with artificial ageing, but there was an increase in corrosion rate. Colvin et al. [13] demonstrated that lithium concentration up to 2.4 wt. % does not significantly affect the electrochemical behaviour of Al–Li(–Ge) alloys. Studies of different forms of corrosion of 8090 Al–Li–Cu–Mg–Zr alloys indicated somewhat superior pitting resistance and stress corrosion cracking (SCC) resistance at least equal to that of the conventional precipitation hardened alloy, although susceptible to exfoliation corrosion [16, 17]. The addition of copper to Al–Li alloys caused corrosion resistance to decrease with ageing and copper addition controlled the SCC resistance [4]. This behavior has been related to the precipitation of the T_1 (Al_2CuLi) phase at the grain boundaries, which is electrochemically very active relative to the grain bodies [18–20]. Thus, although the electrochemical behaviour of the aluminum base alloys has been studied, knowledge of the electrochemical behaviour of Al–Li alloys of

retrogressed and reaged (RRA) temper is scanty. In fact, RRA treatment was initially devised for improving SCC resistance of 7xxx series alloy by Cina [21], but work on RRA characterization and its influence on SCC behaviour of 2xxx and 8xxx series aluminium base alloys have also been carried out by Komisarov et al. and Ghosh et al. [22–24], and it has been found that RRA treatment causes improvement in SCC resistance. This paper deals with the effect of retrogression and reageing (RRA) treatment on the electrochemical behaviour of 8090 and 1441 Al–Li–Cu–Mg–Zr alloys.

2. Experimental details

The 8090 and 1441 Al–Li–Cu–Mg–Zr alloys used in the present study were obtained from the Defence Metallurgical Research Laboratory (DMRL), Hyderabad, India, in sheet form having thickness of 2.8 and 2.0 mm respectively. The sheets of the 8090 alloy were solutionized at 530–535 °C, water quenched, stretched by 1.5–2.5%, followed by artificial ageing at 170 °C for 24 h to the peak aged (T8) temper, whereas the sheets of the 1441 alloy were solutionized at 530–535 °C, water quenched, stretched by 1.5–2.5%, followed by artificial ageing at 150 °C for 4 h and then 170 °C for 24 h to the peak aged (T8) temper. These alloy sheets were aged 170 °C for 96 h to obtain over aged T7 temper. The chemical compositions (wt. %) of the 8090 and 1441 alloys are given in Table 1.

The 8090 and 1441 alloys in the peak aged T8 temper, were subjected to retrogression and reageing (RRA) treatments. Retrogressions were carried out in a small vertical tube furnace in air and the furnace temperatures were maintained within $\pm$ 2 °C of the set value. The retrogression and reaging (RRA) schedule applied to the alloys, discussed elsewhere [22, 23], yielded four RRA tempers of each of the alloys. Electrochemical potentiodynamic polarizations were carried out on 10 mm $\times$ 10 mm coupons of peak aged T8, four RRA T77 and over aged T7 tempers on both alloys using a computer controlled MEINSBERGER potentiostat/galvanostat with inbuilt PS6 software. Experiments were carried out using the standard three electrode configuration: saturated calomel as a reference with a platinum electrode as counter and the sample as the working electrode. Polarisation scans were carried out towards more noble values at a scan rate of 0.5 mV s^{-1}, after allowing a steady state potential to develop. The electrolytes used for the polarization studies were 3.5% NaCl solution, 3.5% NaCl + 0.1M LiCl + 0.3% H_2O_2 solution and 3.5% NaCl + 0.1M LiCl + 0.7% H_2O_2 solutions.

Transmission electron microscopy (TEM), X-ray diffraction (XRD) and differential scanning calorimetry (DSC) studies were carried out to assess the microstructural features and phases of the alloys to explain the electrochemical behaviour. The details of specimen preparation have been discussed elsewhere [22, 23]. A PHILIPS CM12 TEM was used for observation of the microstructures.

X-ray diffraction was carried out for the T8, T7 and T77 RRA tempers of the alloys, using a Philips PW 1710 diffractometer unit with a cobalt as well as a copper target. Differential scanning calorimetry (DSC) runs were initiated from room temperature to 540 °C at a heating rate of 10 °C min^{-1} in an argon atmosphere, using a Stanton Redcroft Model STA 625 (heat flux type) simultaneous thermal analyzer. Specimens of approximately 30 mg were cut from coupons of various tempers and the sides of the specimens were made absolutely flat and smooth for good contact with the crucible during the DSC runs. The output viz. the neat heat flow to the reference (high purity annealed aluminum) relative to the samples was recorded as a function of temperature.

3. Results and discussion

3.1. *Microstructural features*

3.1.1. *TEM observation*

Figures 1(a–c) and 2(a–c) show a few representative TEM photomicrographs of the 8090 and 1441 alloys of different tempers, respectively. TEM microstructural features of the 8090 and 1441 alloys and the influence of RRA treatment on these phases have been discussed in detail by Ghosh et al. and Komisarov et al. [23, 24]. The TEM photomicrographs exhibiting the anodic phases of the alloys that are mostly associated with the observed electrochemical behaviour have been shown in the present paper. Figure 1a, a TEM photomicrograph of the 8090R280DA RRA temper of the 8090 alloy shows uniform distribution of T_1 and S′ precipitates within the matrix and Figure 1(b–c) of the 8090R280IA RRA temper exhibits equilibrium δ phase along the grain and subgrain boundaries. Figure 2a, a TEM image of 1441-T8 temper, exhibits grains containing a uniform distribution of fine T_1 and S′ phases. The micrograph also shows the preferential heterogeneous precipitations of these phases along dislocations within a grain. Equilib-

Table 1. Chemical compositions (in wt. %) of the Al–Li–Cu–Mg–Zr alloys

Alloy	Li	Cu	Mg	Zr	Fe	Si	Al
8090	2.29	1.24	0.82	0.12	0.09	0.044	Balance
1441	1.9	2.0	0.90	0.09	0.11	0.05	Balance

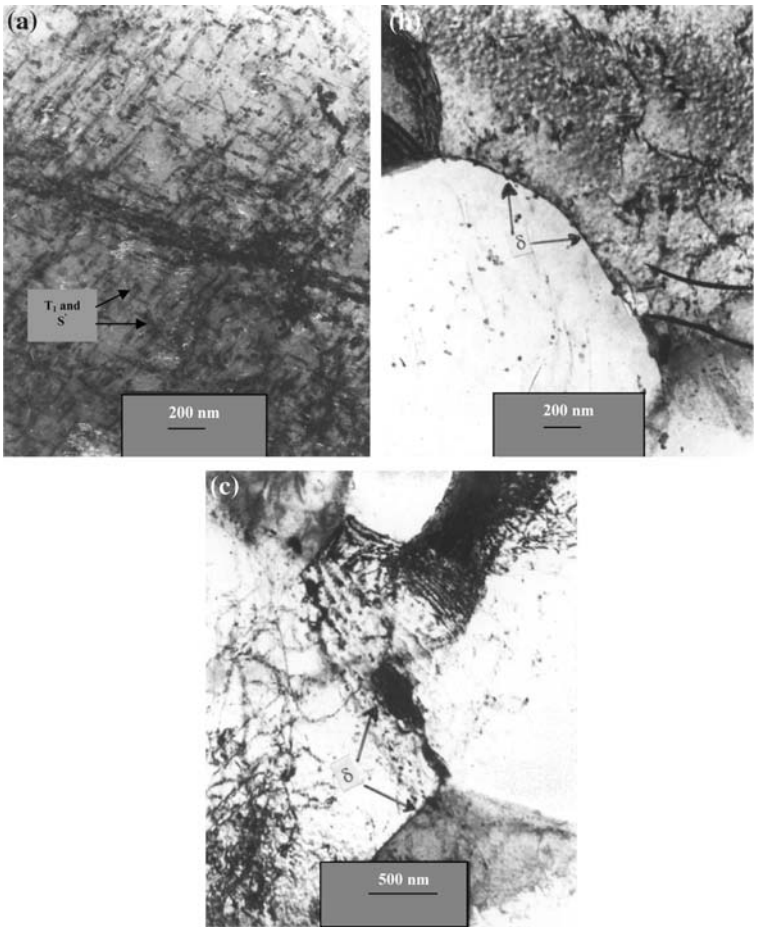

Fig. 1 (a–c). TEM photomicrographs of the 8090 alloy of (a) 8090R280DA temper show uniform distribution of T_1 and S′ precipitates, (b–c) 8090R280IA temper exhibits equilibrium δ phase along the grain and subgrain boundaries.

rium δ phase is also visible at the grain boundaries. Figure 2b, an image of 1441R230DA RRA temper shows equilibrium δ phase along the grain and subgrain boundaries and Figure 2c for the 1441-T7 temper exhibits dense distribution of T_1 and S′ precipitates within the matrix. The occurrence of δ' (Al_3Li) $\rightarrow$ δ (AlLi) phase transformation with the ageing process and RRA treatment results in the enhanced precipitation of δ phase mostly along the grain and subgrain boundaries. The total ageing time of the RRA temper is more than twice to that of the T8 tempers [12–23]. Hence, the observation of enhanced precipitation of δ phase along grain and subgrain boundaries in Figures 1b, c and Figure 2b in the RRA tempers is obvious. With the few TEM micrographs shown here and the detailed TEM studies on these alloys by the authors [22, 23] and others [25, 26] revealed that RRA and over ageing treatment resulted in widespread precipitation of T_1 and S′ phases (Figures 1a and 2c), formation of more and larger equilibrium δ precipitate along grain and as well as on the subgrain boundaries (Figures 1b, 1c and Figure 2b), decrease of dislocation density, generation of more dislocation loops and helices, no alteration of size and distribution of δ' and β' phases, compared to that in the T8 temper of the alloys.

3.1.2. *X-Ray diffractograms*

Figure 3a shows X-ray diffractograms of T8 and RRA tempers of the 8090 alloy using CuK_α radiation. Figure 3b shows X-ray diffractograms of T8, RRA and T7 tempers of the 1441 alloy using CoK_α radiation. The diffractograms of all the tempers show peaks of all the probable phases, δ' (Al_3Li), δ (AlLi), S′ (Al_2CuMg), T_1 (Al_2CuLi) and β' (Al_3Zr) phases that would be present in the alloy system. The diffractograms of the samples of the RRA tempers exhibit the additional $T_{1(102)}$ peak and other intensified peaks of the T_1 and δ phases. During retrogression δ' (Al_3Li) phase dissolves into solution resulting in an increase in lithium content. This increased lithium content causes nucleation and growth of lithium-bearing phases such as T_1 and δ phases and upon reageing the retrogressed state causes reprecipitation of δ' (Al_3Li) phase within the matrix, nucleation of δ phase and growth of the existing T_1 and δ phases.

3.1.3. *DSC thermograms*

Figures 4a and b show the DSC thermograms of the 8090 and 1441 alloys in their T8 and T7 tempers. The exothermic and endothermic peaks in the DSC thermograms representing the sequence of precipitation and

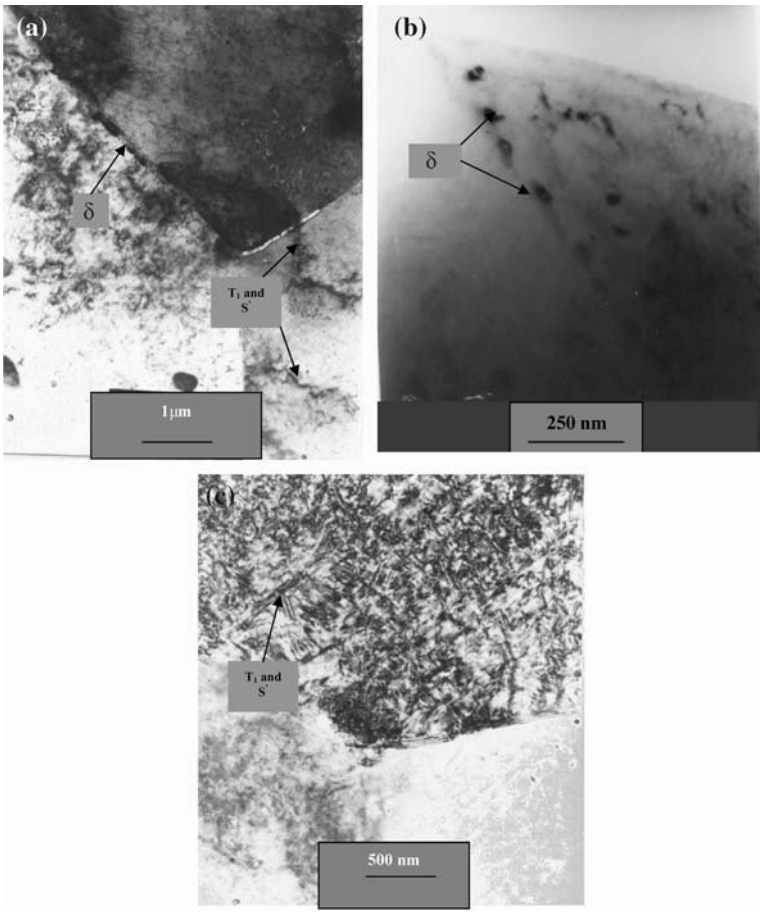

Fig. 2 (a–c). TEM photomicrographs of the 1441-T8 temper (a) show uniform distribution of T_1 and S′ precipitates within the matrix as well as preferentially precipitated along dislocation and also equilibrium δ phase along the grain boundaries, (b) 1441R230DA temper shows equilibrium δ phase along the grain and subgrain boundaries and (c) 1441-T7 temper exhibits dense distribution of T_1 and S′ precipitates within the matrix.

dissolution reactions are well established [27, 28] and are not discussed here. The exothermic peak region D (in Figures 4a and 4b) represents the precipitation of S′ (S), T_1, and δ phases and it should be noted that the higher temperature peak i.e. D_2 is associated with the formation of T_1 and δ phases [28, 29]. For the thermograms of the 8090 alloy (Figure 4a), in the peak region D, the clear appearance of the D_2 peak of the T7 temper as compared to that of the T8 temper indicates that the T7 temper contains a higher proportion of T_1 and δ phases compared to that in the T8 temper. A comparison of Figures 4a and 4b for the T8 tempers of the 8090 and 1441 alloys shows an appearance of two distinct peaks D_1 and D_2 in the peak region D for the 1441 alloy (Figure 4b) which indicates that the precipitation of S′, T_1, and δ phases in these alloys do occur at different temperatures. This is because the 1441 alloy has higher amounts of copper and also the total solute content of the alloys is not the same. Further, for the 1441 alloy, the DSC thermogram of the T7 temper shows that the peak D_2 is of greater intensity (increased magnitude) compared to that of T8 temper. The area under the peak represents the change in enthalpy of formation (ΔH_r) of the precipitates, which is proportional to the volume fractions of the precipitates undergoing reaction. It is apparent from the area under the peak region D, especially of Figure 4b, that the enthalpy of formation (ΔH_r) for the exothermic reaction of the T7 temper is more than that of the T8 temper. This confirms that the T7 temper has higher amounts of T_1, and δ phases compared to that of the T8 temper. This is also confirmed by TEM (Figure 2c) and XRD (Figure 3b).

3.2. *Electrochemical polarization and Alloy tempers*

Potentiodynamic polarization studies were carried out to assess the effect of ageing time and RRA treatment on the electrochemical behaviour of the 8090 and 1441 alloys of various tempers in different environments. Figure 5(a–c) shows the potentiodynamic polarization curves of the 8090 alloy of various (i.e. T8, RRA T77 and T7) tempers in 3.5% NaCl, in 3.5% NaCl + 0.1M LiCl + 0.3% H_2O_2 and in 3.5% NaCl + 0.1M LiCl + 0.7% H_2O_2 solutions. Figure 6(a–c) shows the potentiodynamic polarization curves of the 1441 alloy of various (i.e. T8, RRA T77 and T7) tempers in 3.5% NaCl, in 3.5% NaCl + 0.1M LiCl + 0.3% H_2O_2 and in 3.5% NaCl + 0.1M LiCl + 0.7% H_2O_2 solutions. Tables 2 and 3 give the electrochemical parameters such

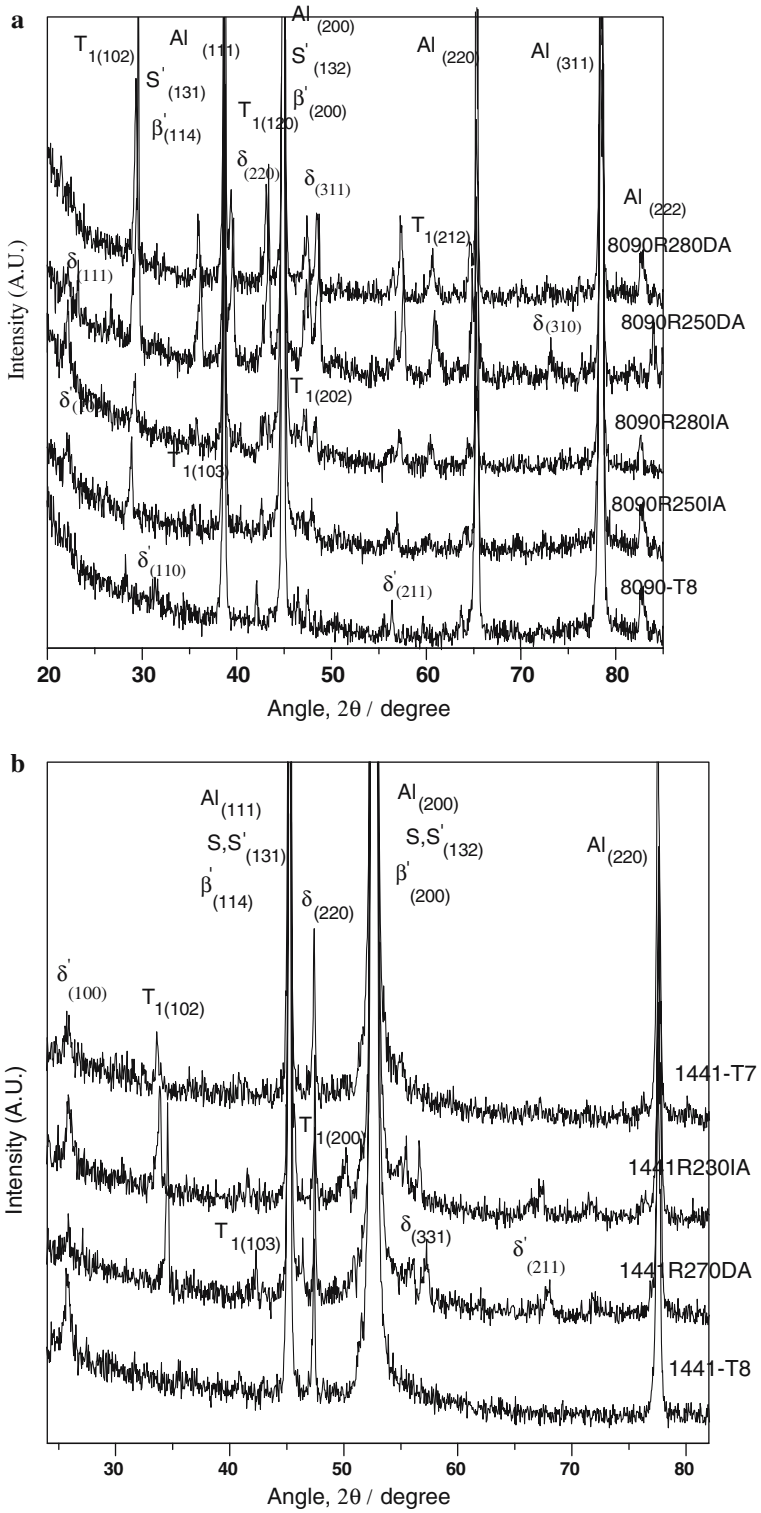

Fig. 3. (a) XRD of the 8090 alloy of various tempers using CuKα radiation. (b) XRD of the 1441 alloy of various tempers using CoKα radiation.

as open circuit potential (OCP), corrosion potential E_{corr} and corrosion rate I_{corr} of the 8090 and 1441 alloys of various tempers, respectively. The corrosion rates and the corrosion potentials were determined by the Tafel extrapolation technique. The corrosion of a heterogeneous alloy depends on the relative areas of exposed phases, the electrode kinetics of each phase and the development and behaviour of local cells. Further, the effects of surface films, grain boundaries, segregation and precipitation and the nature of the electrolyte also come into consideration. Furthermore, each electrochemical reaction may vary with time. Therefore, the prediction and analysis of the electrochemical behaviour of these complex 8090 or 1441 alloys (containing a large number of phases) are extremely difficult [3, 24, 25, 30]. The complexity, in terms of number of phases present in

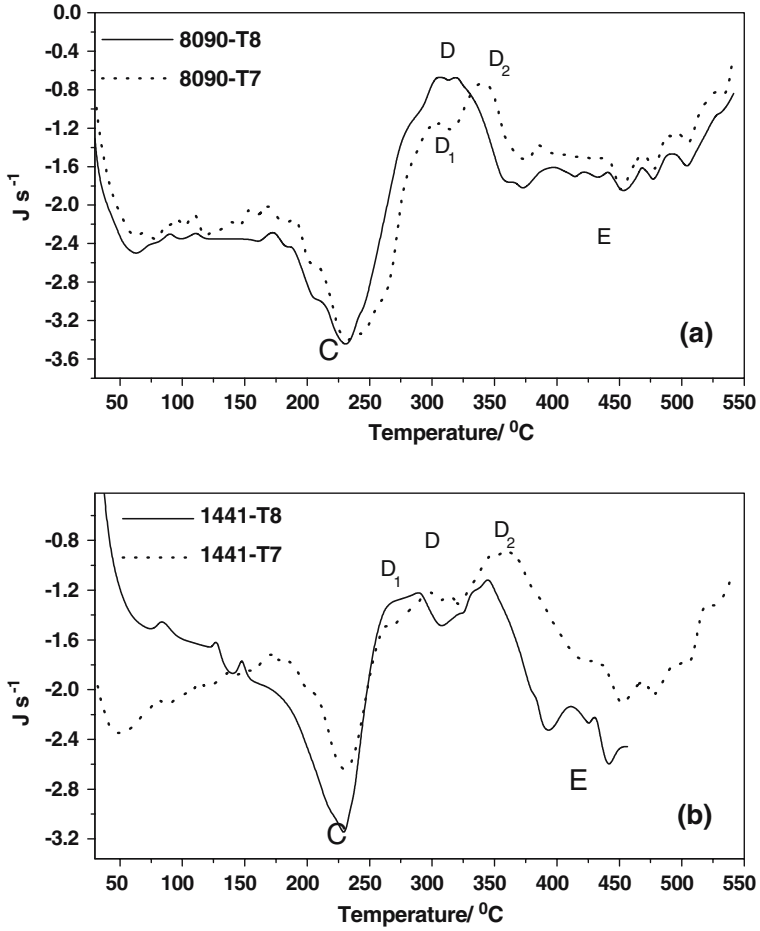

Fig. 4. DSC thermograms of the T8 and T7 tempers of (a) 8090 and (b) 1441 alloys at a heating rate of 10 °C min^{-1}.

the alloy system and the problem of judicious selection of anodic and cathodic Tafel regions impose limitations and therefore the reported E_{corr} and I_{corr} values in Tables 2 and 3 may vary by ± 5%. However, the reported I_{corr} and E_{corr} values in these test environments give an idea of the electrochemical behaviour. The trends of variation in electrochemical parameters with ageing time are consistent with results of other investigators [7, 10–13].

The shape of the polarization curves in Figures 5 and 6 are similar for all tempers of both alloys in all environments. All the polarization curves show only an

Table 2. Electrochemical Data of the 8090 alloy of various tempers in different media

Alloy temper	Environment	OCP vs SCE/mV	I_{corr}/mA cm^{-2}	E_{corr} vs SCE / mV
8090-T8	3.5% NaCl	−725	0.005	−741
	3.5% NaCl + 0.1M LiCl + 0.3% H_2O_2	−688	0.152	−725
	3.5% NaCl + 0.1M LiCl + 0.7% H_2O_2	−670	0.28	−711
8090R280IA	3.5% NaCl	−740	0.012	−794
	3.5% NaCl + 0.1M LiCl + 0.3% H_2O_2	−732	–	–
	3.5% NaCl + 0.1M LiCl + 0.7% H_2O_2	−694	0.358	−717
8090R280DA	3.5% NaCl	−731	0.004	−763
	3.5% NaCl + 0.1M LiCl + 0.3% H_2O_2	−710	–	–
	3.5% NaCl + 0.1M LiCl + 0.7% H_2O_2	−667	0.243	−706
8090R250IA	3.5% NaCl	−734	0.008	−789
	3.5% NaCl + 0.1M LiCl + 0.3% H_2O_2	−715	–	–
	3.5% NaCl + 0.1M LiCl + 0.7% H_2O_2	−690	0.389	−703
8090R250DA	3.5% NaCl	−736	0.006	−786
	3.5% NaCl + 0.1M LiCl + 0.3% H_2O_2	−717	0.122	−743
	3.5% NaCl + 0.1M LiCl + 0.7% H_2O_2	−680	0.201	−710
8090-T7	3.5% NaCl	−752	0.016	−833
	3.5% NaCl + 0.1M LiCl + 0.3% H_2O_2	−732	0.167	−769
	3.5% NaCl + 0.1M LiCl + 0.7% H_2O_2	−693	0.328	−705

Open circuit potential (OCP) is the potential at the zero current from the potentiodynamic curves. I_{corr} is the current density (mA cm^{-2}) and E_{corr} is the potential (mV, SCE) at I_{corr}.

Table 3. Electrochemical Data of the 1441 alloy of various tempers in different media

Alloy temper	Environment	OCP vs SCE / mV	I_{corr}/mA cm^{-2}	E_{corr}vs SCE / mV
1441-T8	3.5% NaCl	− 697	0.07	− 760
	3.5% NaCl + 0.1M LiCl + 0.3% H_2O_2	− 660	0.298	− 674
	3.5% NaCl + 0.1M LiCl + 0.7% H_2O_2	− 615	0.340	− 639
1441R270IA	3.5% NaCl	− 732	0.006	− 750
	3.5% NaCl + 0.1M LiCl + 0.3% H_2O_2	− 709	0.088	− 722
	3.5% NaCl + 0.1M LiCl + 0.7% H_2O_2	− 651	0.545	− 664
1441R270DA	3.5% NaCl	− 718	0.013	− 770
	3.5% NaCl + 0.1M LiCl + 0.3% H_2O_2	− 649	0.189	− 678
	3.5% NaCl + 0.1M LiCl + 0.7% H_2O_2	− 627	–	–
1441230IA	3.5% NaCl	− 727	0.005	− 751
	3.5% NaCl + 0.1M LiCl + 0.3% H_2O_2	− 707	0.23	− 727
	3.5% NaCl + 0.1M LiCl + 0.7% H_2O_2	− 641	0.37	− 660
1441R230DA	3.5% NaCl	− 728	0.0025	− 732
	3.5% NaCl + 0.1M LiCl + 0.3% H_2O_2	− 712	0.140	− 756
	3.5% NaCl + 0.1M LiCl + 0.7% H_2O_2	− 635	0.330	− 653
1441-T7	3.5% NaCl	− 743	0.019	− 786
	3.5% NaCl + 0.1M LiCl + 0.3% H_2O_2	− 723	0.105	− 737
	3.5% NaCl + 0.1M LiCl + 0.7% H_2O_2	− 646	0.622	− 676

Open circuit potential (OCP) is the potential at the zero current from the potentiodynamic curves. I_{corr} is the current density (mA cm^{-2}). E_{corr} is the potential (mV, SCE) at I_{corr}.

active region with no distinct passive region. The absence of passive regions is because OCP values are around or beyond the pitting potential. The pitting potentials (E_p) of these alloys have been found to be around − 725.7 mV (SCE) and − 730.0 mV (SCE) in 3.5% NaCl solution and in 3.5% NaCl + 0.1M LiCl solution, respectively. The pit generation potential (E_p) for the alloy system is calculated according to the following empirical relation given by [31];

$$E_p(\text{mV/SCE}) = -740 - 64\log[Cl^-] \quad (1)$$

The calculated pitting potentials are in close agreement with reported values [11]. The polarization curves of 8xxx series alloys exhibited a passive region in the potential range − 1100 to − 700 mV (SCE) in alkali solutions and the OCP is around − 1200 mV [32]. The absence of a passive region in our observation (Figures 5 and 6) suggests that the associated oxide films are not stable. The main factors controlling the stability of the oxide film are the potential of the alloy and the concentrations of metallic and hydroxyl ions. Aqueous solutions of halides are known to be aggressive and to retard film repair and they are known to cause pitting in these alloys. Ambat et al. [33] state that the effect of chloride ion concentration on corrosion rate is found to be greater at neutral pH, compared with that in highly acidic and alkaline solutions. The dissolution of aluminium in neutral environments may be described by the following reactions.

$$Al^{3+} + H_2O = AlOH^{2+} + H^+ \quad (2)$$

$$Al^{3+} + 2H_2O = Al(OH)_2^+ + 2H^+ \quad (3)$$

$$Al^{3+} + 3H_2O = Al(OH)_3 + 3H^+ \quad (4)$$

At neutral pH the concentration of OH^- ions is comparatively low at $\sim 10^{-7}$ mol l^{-1} and solutions containing chloride ions can accelerate corrosion by attacking the oxide film. The presence of oxygen in the solution facilitates other cathodic reactions and also plays an important role in the rate of corrosion, which is discussed in the subsequent section.

Further, the polarization curves (Figures 5 and 6) and Tables 2 and 3 show that the OCP values have shifted negatively (anodically) with RRA treatment and ageing time and this has been observed in all the test environments. The OCP values of the T7 tempers of both alloys are the most negative, whereas the OCP values of the RRA tempers lie in between that of the T7 and T8 tempers. In general, in a given electrolyte, the OCP value depends on the microstructure and the constituent alloy phase [9, 10, 34].

The greater negative shift of OCP for the RRA and over aged T7 tempers compared to the peak aged temper is due to the presence of higher amounts of δ, T_1 and S′(S) phases which are anodic in nature [20, 35], as confirmed by our TEM, XRD and DSC studies (Figures 1–4). The negative shift in potential in all electrolytes for all tempers can also be attributed to a gradual establishment of microscopic galvanic local cell formation. The greater the ageing time, the greater is the precipitation of T_1 and δ phase within the grains, along the grain boundaries and on the subgrain boundaries, giving sites for local cell formation.

Tables 2 and 3 indicate that the corrosion rate is more or less the same for all the tempers in 3.5% NaCl solution, but the corrosion potential (E_{corr}) shifts in the negative direction with aging time and RRA treatment. Similar observations have also been reported [7, 10, 11, 32]. Further, a comparison of Figures 5 and 6 and

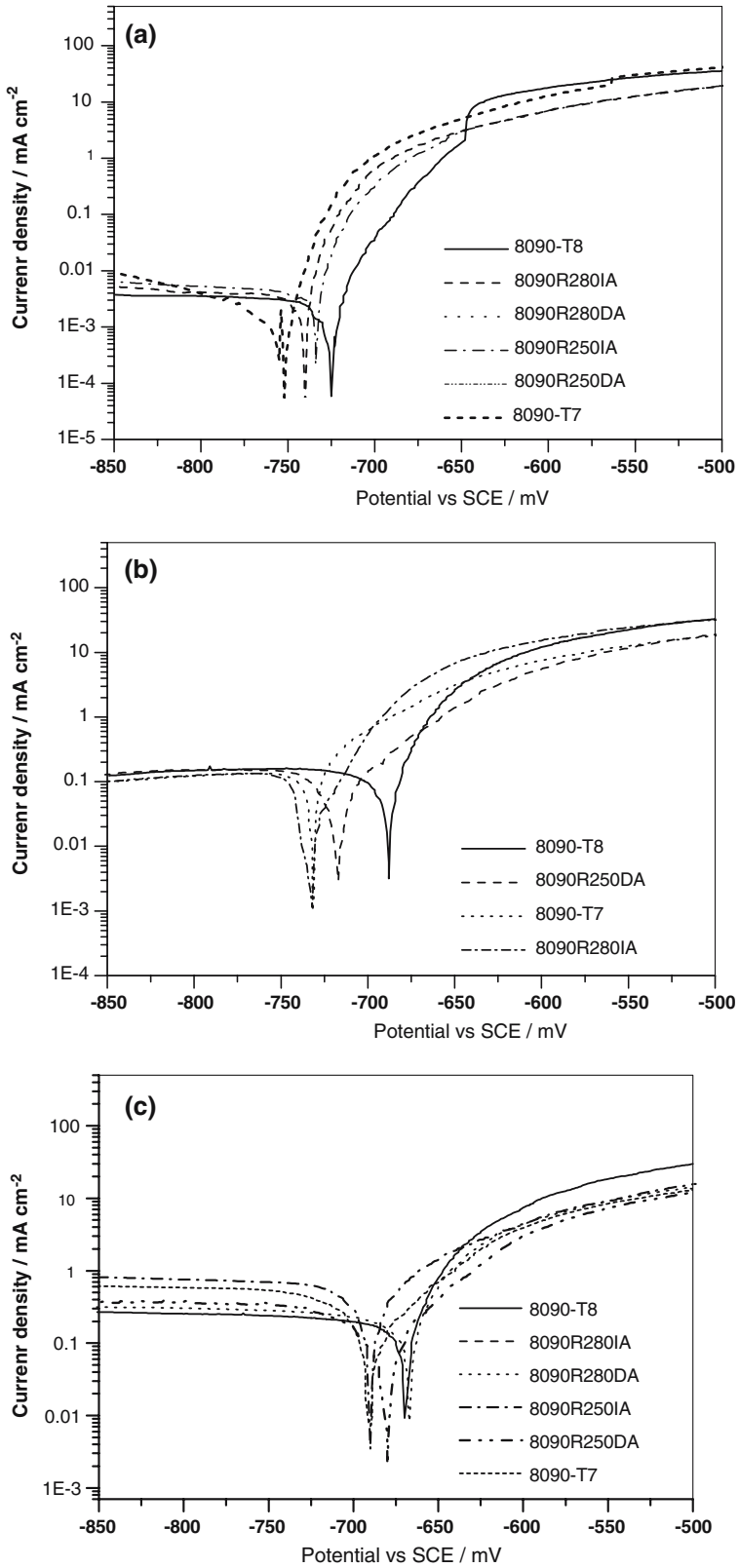

Fig. 5 (a–c). Potentiodynamic polarisation curves of the 8090 alloy of various tempers in (a) 3.5% NaCl, (b) 3.5% NaCl + 0.1M LiCl + 0.3% H_2O_2 and (c) 3.5% NaCl + 0.1M LiCl + 0.7% H_2O_2 solutions at a scan rate of 0.5 mVs^{-1}.

Tables 2 and 3 also indicates that the OCP values of the 1441 alloy of T8 and other tempers are more positive (noble) to that of the 8090 alloy for the corresponding tempers. This is attributable to the presence of a higher amount of copper in the 1441 alloy with respect to 8090, as copper is one of the

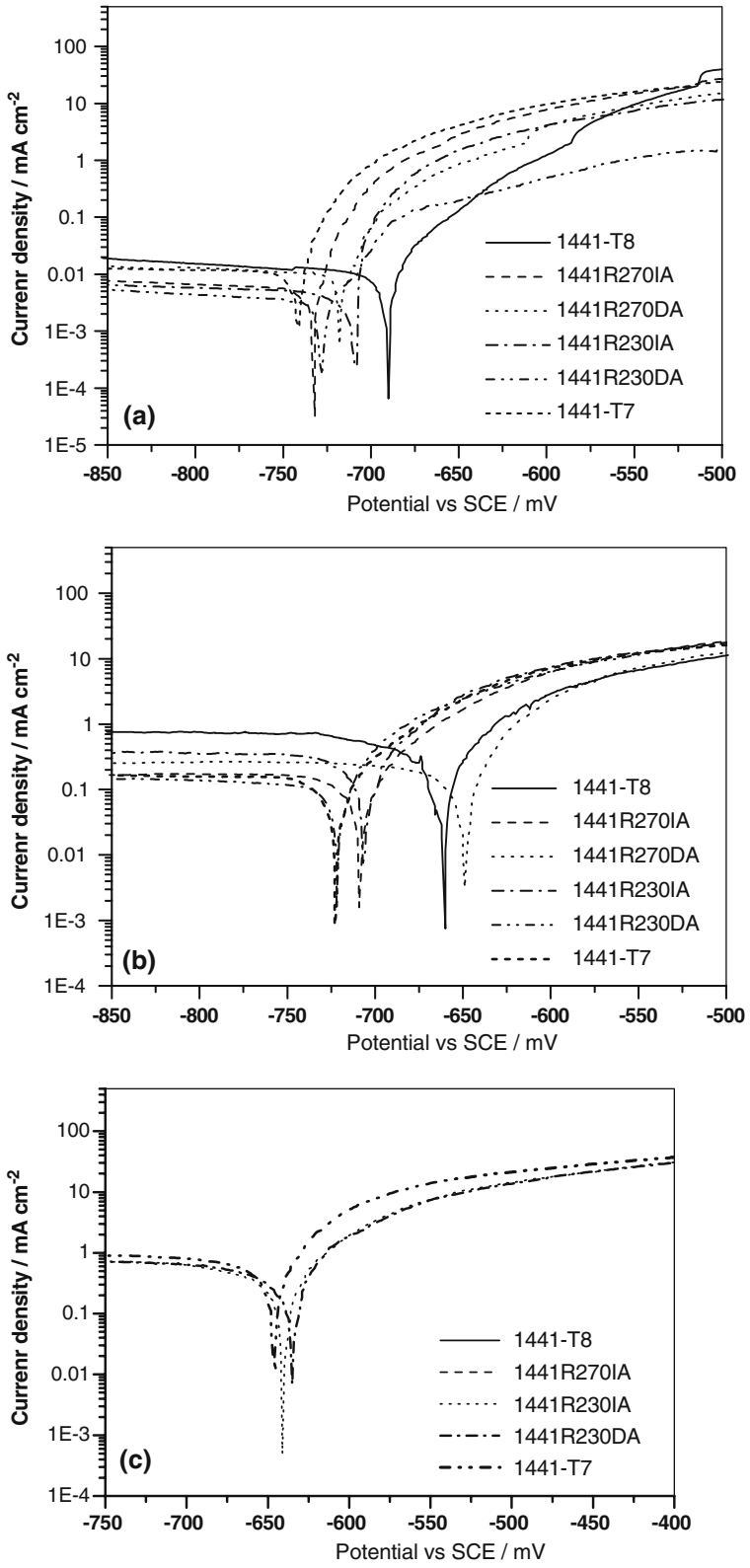

Fig. 6 (a–c). Potentiodynamic polarisation curves of the 1441 alloy of various tempers in (a) 3.5% NaCl, (b) 3.5% NaCl + 0.1M LiCl + 0.3% H_2O_2 and (c) 3.5% NaCl + 0.1M LiCl + 0.7% H_2O_2 solutions at a scan rate of 0.5 mVs^{-1}.

elements that shift the potential in the noble direction when added to aluminum [36]. In general, the effect of multiple elements in solid solution on OCP is approximately additive. Further, in the case of Al–Li alloys, the electrochemical potential is independent of lithium additions up to 3% and there is no difference in corrosion potential between alloys containing lithium and those not containing lithium [37].

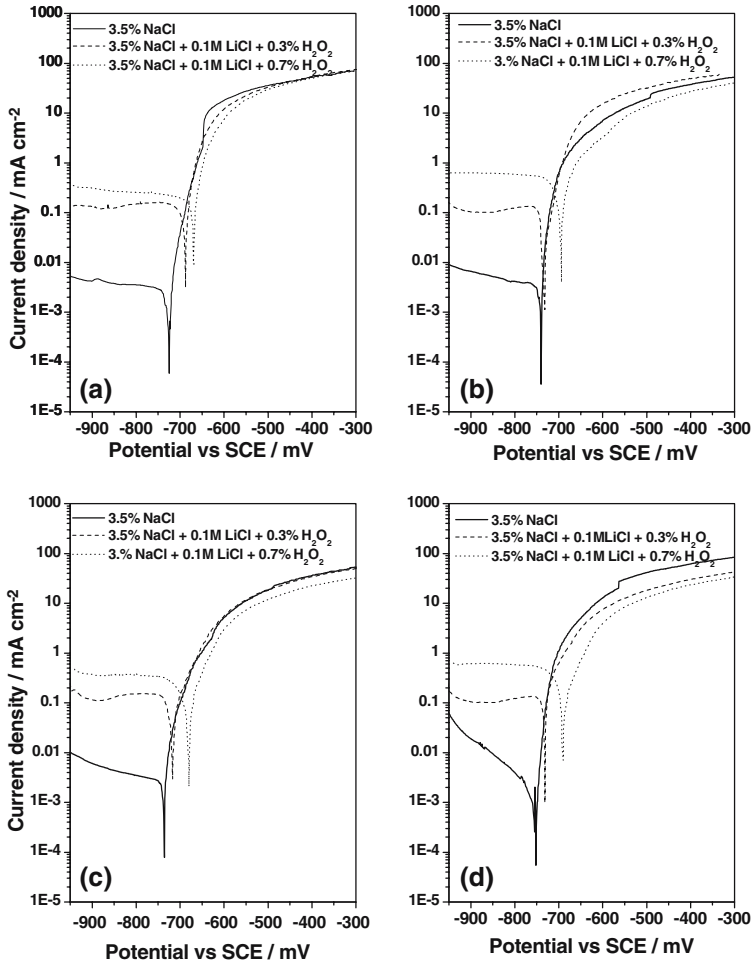

Fig. 7 (a–d). Potentiodynamic polarisation curves of (a) 8090-T8 (b) 8090R2801A, (c) 8090R250DA, and (d) 8090-T7 in different environments at a scan rate of 0.5 mVs^{-1}.

3.3. *Electrochemical polarization and Environments*

Figure 7(a–d) shows the potentiodynamic polarization curves in 3.5% NaCl, 3.5% NaCl + 0.1M LiCl + 0.3% H_2O_2 and 3.5% NaC + 0.1M LiCl + 0.7% H_2O_2 solutions of the 8090 alloy of T8, RRA 8090R280IA, 8090R250DA and T7 tempers, respectively. Similarly, Figure 8(a–d) shows the potentiodynamic polarization curves in 3.5% NaCl, 3.5% NaCl + 0.1M LiCl + 0.3% H_2O_2 and 3.5% NaCl + 0.1M LiCl + 0.7% H_2O_2 solutions of the 1441 alloy of T8, RRA 1441R270IA, 1441R230DA and T7 tempers, respectively.

There is a cathodic shift of OCP values with the addition of LiCl and H_2O_2 in 3.5% NaCl solution. The greater the H_2O_2 addition the greater is the shift of OCP. The aggressive depassivating nature of the 3.5% NaCl solution makes the alloy bare, but the addition of H_2O_2 maintains the passive oxide layer or heals the destroyed oxide layer, which shifts the OCP in the cathodic direction. In the cathodic region there is an increase of current density in 3.5% NaCl + 0.1M LiCl + 0.3% H_2O_2 and in 3.5% NaCl + 0.1M LiCl + 0.7% H_2O_2 solution compared to that in 3.5% NaCl. Thus, in all the tempers for both alloys, the position of the cathodic curves in solution containing LiCl and H_2O_2 have shifted to higher current density values, although the slopes remain the same. This may be due to the fact that the presence of oxidizing agent i.e. H_2O_2 in NaCl solution, facilitates cathodic reactions that enhance the corrosion rate. In the anodic region for all alloy tempers, although the current density is initially higher in environments containing LiCl and H_2O_2 compared to that in 3.5% NaCl, the curves tend to converge at higher potential corresponding to the high value of current density. The difference in E_p (pitting potential) and OCP values of the environments containing LiCl and H_2O_2 is more than that in 3.5% NaCl. Thus, environments containing LiCl and H_2O_2 are more aggressive for localized attack than 3.5% NaCl solution alone.

4. Conclusions

Microstructural evaluation of both 8090 and 1441 alloys by TEM, XRD and DSC studies have revealed all the probable phases, such as δ' (Al_3Li), δ (AlLi), S′

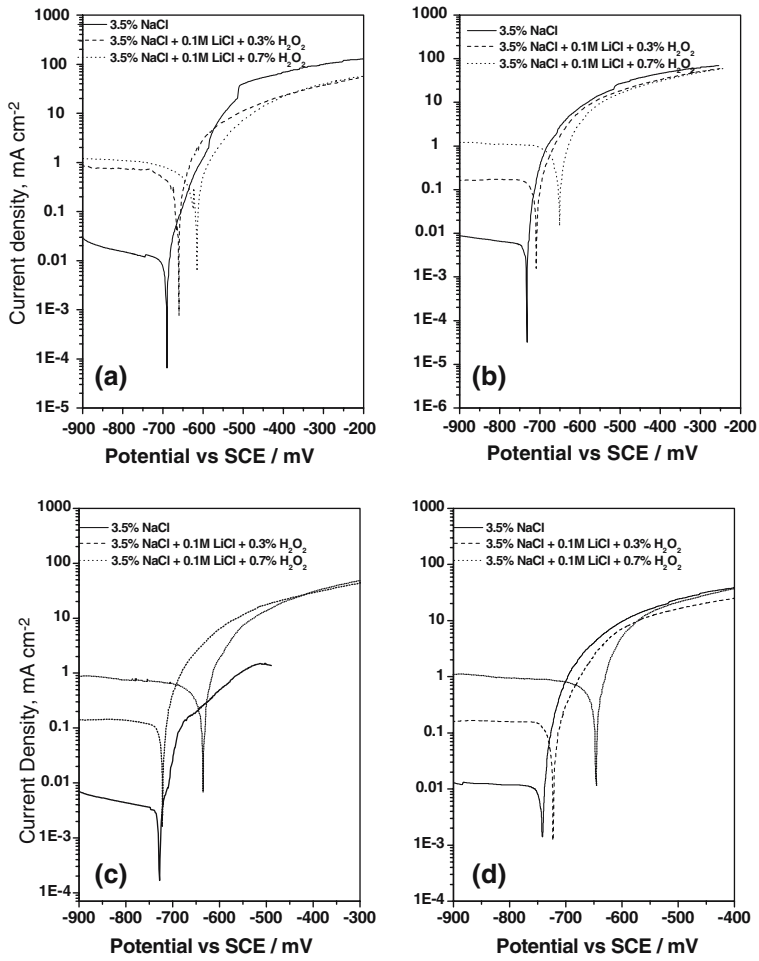

Fig. 8 (a–d). Potentiodynamic polarisation curves of (a) 1441-T8 (b) 1441R2701A, (c) 1441R230DA, and (d) 1441-T7 in different environments at a scan rate of 0.5 mVs^{-1}.

(Al_2CuMg), T_1 (Al_2CuLi) and β' (Al_3Zr), to be present in the alloy system. Diffractograms of the RRA tempers exhibited an additional peak and intense peaks of T_1 and δ phases for the RRA tempers. TEM photomicrographs show that RRA and over aged tempers contain enhanced precipitation S′ and T_1 precipitates in the matrix and equilibrium δ phase precipitation on the grain and sub-grain boundaries. DSC thermograms of the T7 tempers of both alloys exhibit enhanced D_2 peak of T_1 and δ phases and also indicate higher amounts of δ phase as compared to T8 tempers.

Electrochemical polarization studies indicated that the OCP values of the RRA tempers for both alloys lie between the OCP values of the T8 and T7 tempers, but the corrosion rate in a given environment is more or less the same irrespective of the temper. The OCP values shifted negatively (anodically) with ageing time and RRA treatment. This is consistent with the precipitation of higher amounts of anodic phases such as δ, S′ and T_1, which has been confirmed by TEM, XRD and DSC studies. Therefore, based on the microstructural features and the observed electrochemical behaviour, it is to be concluded that the microstructures of the RRA tempers approach those of the T7 temper.

Acknowledgements

The authors thank Dr. A. A. Gokhale and Dr. Vijaya Singh, Scientist, Defence Metallurgical Research Laboratory (DMRL), Hyderabad, India for providing the alloys.

References

1. J.R. Davis *et al.*, *ASM Specialty Handbook, Aluminum and Aluminum Alloys, ASM International* (The Materials Information Society, Ohio, 1998).
2. M. Ahmad and T. Ericsson. *in* C. Baker, P.J. Gregson, S.J. Harris and C.J. Peel (eds), Aluminum Lithium III, Proc. 3rd Int. Conf. on Aluminum Lithium Alloys, (The Institute of Metals, London, 1986), p. 509.
3. J.G. Rinkers, M. Marek and T.H. Sanders Jr., *J. Mater Sci.* **64** (1984) 203.
4. N.J.H. Holroyd, A. Gray, G.M. Scamans and R. Hermann. *in* C. Baker, P.J. Gregson, S.J. Harris and C.J. Peel (eds), Aluminum Lithium III, Proc. 3rd Int. Conf. on Aluminum Lithium Alloys, (The Institute of Metals, London, 1986), p. 310.
5. F. Binsfeld, M. Habashi, J. Galland, J.P. Fidelle, D. Minnay and P. Rofidal, *in* G. Champier, B. Dubost, D. Miannay, L. Sabetay and J. de Physique (Eds), Aluminum Lithium IV, Proc. 4th Int

Aluminum Lithium Conf. Colloque C3, supplement, 48 (1987) C3: 587.
6. A. Conde and J.J. Damaborenea, *Corros. Sci.* **41** (1999) 1079.
7. A. Gray, (1987) Aluminium–Lithium IV, Proc. 4th Int. Conf. on Aluminum-Lithium Alloys. *J de Physique Colloque*, C3, supplement, 48 C3: 891.
8. M.O. Speidel, *Metallurg. Trans. A* **6A** (1975) 631.
9. A. Roth and H. Kaesche. *in* T.H. Sanders Jr. and E.A. Starke Jr. (eds), Aluminum Lithium V, Proc. 5th Int. Aluminum Lithium Conf., (Materials and Component Engineering Publications (MCEP), Warrendale, PA, 1989), p. 1197.
10. J.M. Sater and T.H. Sanders, ibid, p. 1217.
11. B. Bavarian, J. Becker, S.N. Parikh and M. Zamanzadeh, ibid, p. 1227.
12. T.S. Srivatsan, G.E. Bobeck, T.S. Sudarshan and P.A. Molian, ibid, p. 1237.
13. E.L. Colvin, G.L. Cohen Jr., G.E. Stoner and E.S. Starke Jr., *Corrosion* **42** (1986) 416.
14. R.E. Ricker and D.J. Duquette. *in* C. Baker, P.J. Gregson, S.J. Harris and C.J. Peel (eds), Aluminum Lithium III, Proc. 3rd Int. Conf. on Aluminum Lithium Alloys, (The Institute of Metals, London, 1986), p. 581.
15. H.F. De Jong and J.H.M. Martens, *Aluminium* **61** (1985) 416.
16. P.L. Plane, J.A. Gray and C.T.E. Smith. *in* C. Baker, P.J. Gregson, S.J. Harris and C.J. Peel (eds), Aluminum Lithium III, Proc. 3rd Int. Conf. on Aluminum Lithium Alloys, (The Institute of Metals, London, 1986), p. 273.
17. M.A. Reynolds, A. Gray, E.E. Greed, R.M. Jordan and A.A. Titchener, ibid, 57.
18. E.I. Meletis and Huang Weiji, *Mat. Sci. Engg. A* **148** (1991) 197.
19. E.I. Meletis, *Mat. Sci. Engg. A* **93** (1987) 235.
20. R.G. Buchheit and G.E. Stoner. *in* T.H. Sanders Jr. and E.A. Starke Jr. (eds), Aluminum Lithium V, Proc. 5th Int. Conf. Aluminum Lithiu, (MCEP, Warrendale, PA, 1989), p. 1347.
21. B. Cina, US Patent, No. 3856584, December 24, 1974.
22. K.S. Ghosh, K. Das and U.K. Chatterjee, *Metal. Mat. Trans. A* **36A** (2005) 3477.
23. K.S. Ghosh, K. Das and U.K. Chatterjee, *Mat. Sci. Tech.* **20** (2004) 825.
24. V. Komisarov, M. Talianker and B. Cina, *Mater. Sci. Engg. A* **A221** (1996) 113.
25. H.M. Flower and P.J. Gregson, *Mat. Sci. Tech.* **3** (1987) 81.
26. V. Komisarov, M. Talianker and B. Cina, *Mater. Sci. Engg. A* **A242** (1998) 39.
27. A. Luo, D.J. Lloyd, A. Gupta and W.V. Youdelis, *Acta Metal. Mater.* **41** (1993) 769.
28. A.K. Mukhopadhyay, C.N.J. Tite, H.M. Flower, P.J. Gregson and F. Sale, *in* G. Champier, B. Dubost, D. Miannay, L. Sabetay, (Eds.), Aluminum Lithium IV, Proc. 4th Int. Aluminum Lithium Conf., *J de Physique*, Supplement, 48 (1987) p. C3:439.
29. S. Ozbilen and H.M. Flower. *in* T.H. Sanders Jr. and E.A. Starke Jr. (eds), Aluminum Lithium V, Proc. 5th Int. Aluminum Lithium Conf, (MCEP, Warrendale PA, 1989), p. 651.
30. J.G. Rinker, M. Marek and T.H. Sanders Jr.. *in* T.H. Sanders Jr. and E.A. Starke Jr. (eds), Proc. 2nd Int. Conf. on Aluminum-Lithium II, (TMS, Warrendale, 1984), p. 597.
31. S. Schnuriger, G. Mankowski, Y. Roques, G. Chatainier and F. Dabosi, *in* G. Champier, B. Dubost, D. Miannay and L. Sabetay, (Eds), Aluminum Lithium IV, Proc. 4th Int. Aluminum Lithium Conf., *J de Physique*, Supplement, 48 (1987) p. C3: 851.
32. R. Ambat and E.S. Dwarakdasa, *J. Appl. Electrochem.* **24** (1994) 911.
33. R. Ambat and E.S. Dwarakdasa, *British. Corros. J.* **28** (1993) 141.
34. R.H. Jones and R.E. Ricker, (1992) *in* R.H. Jones (Eds), Stress Corrsion Cracking: Mechanisms and Evaluation. ASM International, 1992.
35. J. Garcia, P. Ponthiaux, M. Habashi, Galland J. *in* G. Champier, B. Dubost, D. Miannay and L. Sabetay (Eds), Aluminum Lithium IV, Proc. 4th Int. Aluminum Lithium Conf., *J de Physique*, Supplement, 48 (1987) p. C3:861.
36. J.G. Rinker, M. Marek and T.H. Sanders. *in* T.H. Sanders Jr. and E.A. Starke Jr. (eds), Aluminum Lithium V, Proc. 5th Int. Conf. Aluminum Lithium, (MCEP, Warrendale, PA, 1989), p. 597.
37. M. Reboul and P. Meyer *in* G. Champier, B. Dubost, D. Miannay and L. Sabetay (Eds), Aluminum Lithium IV, Proc. 4th Int. Aluminum Lithium Conf. *J de Physique*, Supplement, 48 (1987) p. C3:881.